# Spacetime thermodynamics and subsystem observables in a kinetically constrained model of glassy systems

Robert L. Jack,[1,2] Juan P. Garrahan,[3] and David Chandler[2]

[1] *Rudolf Peierls Centre for Theoretical Physics, University of Oxford, 1 Keble Road, Oxford, OX1 3NP, UK*
[2] *Department of Chemistry, University of California, Berkeley, CA 94720-1460*
[3] *School of Physics and Astronomy, University of Nottingham, Nottingham, NG7 2RD, UK*

In a recent article [M. Merolle et al., Proc. Natl. Acad. Sci. USA 102, 10837 (2005)] it was argued that dynamic heterogeneity in $d$-dimensional glass formers is a manifestation of an order-disorder phenomenon in the $d+1$ dimensions of spacetime. By considering a dynamical analogue of the free energy, evidence was found for phase coexistence between active and inactive regions of spacetime, and it was suggested that this phenomenon underlies the glass transition. Here we develop these ideas further by investigating in detail the one-dimensional Fredrickson-Andersen (FA) model in which the active and inactive phases originate in the reducibility of the dynamics. We illustrate the phase coexistence by considering the distributions of mesoscopic spacetime observables. We show how the analogy with phase coexistence can be strengthened by breaking microscopic reversibility in the FA model, leading to a non-equilibrium theory in the directed percolation universality class.

## I. INTRODUCTION

The hallmarks of the glass transition [1] are a sudden increase of relaxation times, and dynamic heterogeneity [2]. A recent paper [3] described the idea that these phenomena are manifestations of phase coexistence in spacetime. The two competing phases are an active state, where dynamics is plentiful, and an inactive one, where dynamics is scarce. The purpose of the current paper is to develop these ideas by building on the results of Ref. [3].

In the active phase of the dynamics, the existence of the nearby inactive phase can be inferred by measuring the distribution of any observable that quantifies dynamics within a finite spacetime window [3]. These distributions display non-Gaussian tails, because of the coexisting inactive phase. This is analogous to the situation in standard phase transitions: the distribution of cavity sizes in a fluid near liquid vapour coexistence has non-Gaussian tails [4], as does the distribution of box magnetization for the Ising model in the vicinity of its phase transition. [5].

The concept of *spacetime thermodynamics* [3] is illustrated in Fig. 1. A simple picture of glassy dynamics at low temperatures is that of diffusing excitations, which coalesce and branch. This dynamics is reducible [6]. That is, there are two steady states, an active one with a finite density of excitations (the "equilibrium" state), and an inactive one with strictly zero density. Working in the equilibrium state, the dominant fluctuations on large length scales are spacetime regions in which there are no excitations, as illustrated in Fig. 1. We refer to these regions as "bubbles" of the inactive phase. As mentioned above, the statistics of these rare fluctuations are similar to those at liquid-vapour phase coexistence.

Motivated by this correspondence, we characterise the bubbles by the probability density function $P_{\rm bubble}(l,\tau)$ for their spatial and temporal extents (denoted $l$ and $\tau$, respectively). For bubbles which are large compared with the bulk correlation length of the active state we can write:

$$P_{\rm bubble}(l,\tau) \propto \exp\left\{-\left[\sigma_1 l + \sigma_2 \tau + \mu l\tau + \Lambda(l-v\tau)^2\right]\right\}, \quad (1)$$

where $\sigma_{1,2}$ are "surface tensions" in the spatial and temporal directions, $\mu$ is the "free energy" difference between active and inactive phases, and $\Lambda$ controls the aspect ratio of the bubbles, in conjunction with the velocity parameter $v$. The bubble free energy can be investigated by considering the probability distribution functions for observables that are averaged over finite regions of spacetime, such as the boxes in Fig. 1 [3]. The tails of these distributions are dominated by large rare bubbles which extend over many correlation lengths of the active state.

We associate the distribution of bubble sizes with a (spacetime) free energy that we sketch as a function of excitation density in Fig. 2, where we show schematically the effect of the surface tension and chemical potential-like terms. The free energy has two minima, associated with the active and inactive states. If the free energy difference $\mu = 0$, the system lies on a phase coexistence line. The key point is that this situation coincides with the reducibility of the dynamics; specifically, a boundary condition suffices to make the system choose one phase. For example, consider a system with periodic spatial boundary conditions, as sketched in Fig. 2. If we choose our initial condition to be the empty lattice, then this inactive state persists forever; all other initial conditions lead to the active state.

To expand on these ideas, we use the Fredrickson-Andersen (FA) facilitated spin model [7] as an illustrative system. We analyze the distributions of spacetime observables, such as the total amount of dynamical activity inside a given spatial region, integrated over a finite observation time. We use the forms of these distributions to demonstrate the coexistence between active and inactive phases.

It is instructive to compare the FA model with two other systems. In Ref. [8], a model with appearing and

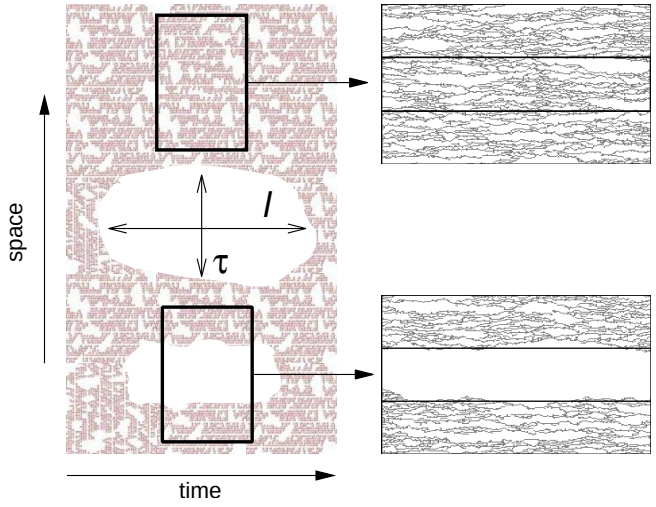


FIG. 1: Illustration of a trajectory in a facilitated model with spacetime "bubbles" of the inactive state. The boxes illustrate finite observation spacetime windows: the top one corresponds to a typical region; the bottom one is a rare collective fluctuation of size much larger than those typical of the active state. On the right are actual trajectories from the FA model at $T = 1$ for observation windows of $L = 180$ and $t_{\rm obs} = 320$ (smaller observation windows of $L = 60$ are also outlined).

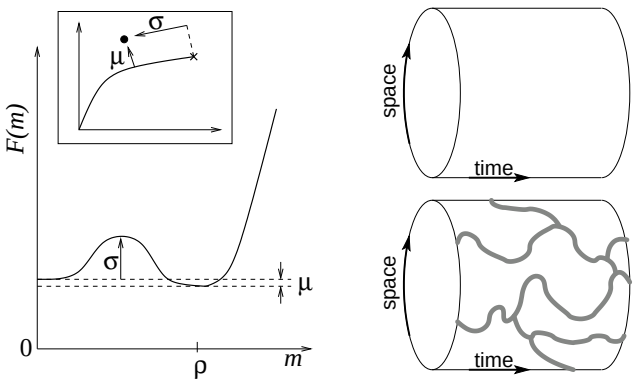


FIG. 2: (Left) Sketch of the free energy of trajectories as a function of excitation density $m$, resembling the situation near a first order phase transition. The minima at $m = \rho$ and $m = 0$ correspond to the active and inactive states, respectively. The parameters $\mu$, $\sigma$ and $\rho$ are the bulk free energy difference, bubble surface tension and order parameter, respectively. The inset is a schematic "phase diagram" with a first order line separating the active and inactive phases and ending in a critical point. The chemical potential difference $\mu$ measures the distance from the first order line, while the surface tension $\sigma$ that from the critical point. (Right) Imposing periodic boundary conditions in space leads to a cylindrical spacetime region where the spatial coordinate runs around the cylinder. We illustrate how the reducibility of the dynamics leads to a qualitative effect of the boundary conditions on the bulk behaviour: an initial state with no excitations remains inactive forever, while an initial state with any finite number of excitations remains active forever. The choice of boundary condition affects the bulk properties of the system, regardless of its extent: this is a signature of phase coexistence.

annihilating excitations (the so-called AA model) was shown to have the same two point correlations as the FA model (up to a multiplicative factor). However, the AA model lacks a stable inactive phase, and there is no spacetime phase coexistence. We demonstrate this by considering the statistics of bubbles in that model. We conclude that phase coexistence is a collective effect that does not appear in two point functions. Conversely, if microscopic reversibility is broken in the FA model then the system moves into the directed percolation universality class [9] and the two point functions and critical scaling change qualitatively. However, the non-equilibrium model still exhibits spacetime phase coexistence (between active and absorbing states). In fact, the phase coexistence is more easily observed in the resulting non-equilibrium steady state than in the FA model at equilibrium. For this reason, we argue that phase coexistence phenomena might be more easily observed in driven glassy systems than in equilibrium states.

The paper is organized as follows. In section II we define the model, discuss its trajectories, and introduce the observables of interest. We also show that reducibility of the dynamics is essential to see the phase coexistence effect. In section III we formalise our discussion of spacetime thermodynamics by considering the distribution of the dynamical action that is analogous to the thermodynamic free energy. We consider the effect of breaking microscopic reversibility in section IV.

## II. MODEL, TRAJECTORIES AND OBSERVABLES

Kinetically constrained models (see Ref. [6] for a comprehensive review) are defined in such a way that their non-trivial behaviour is purely dynamical in origin. Thus, they are the natural framework for investigating dynamical heterogeneity and its consequences [10, 11, 12, 13, 14, 15]. The simplest kinetically constrained model of all is the single-spin facilitated FA model [6, 7] in dimension $d = 1$. It is defined for a chain of $N$ binary variables $n_i \in \{0, 1\}$, with trivial Hamiltonian $H = -J \sum_i n_i$. The model evolves under the following Monte-Carlo (MC) dynamics. At each MC iteration a randomly chosen site $i$ changes state according to:

$$n_i = 0 \;\rightarrow\; n_i = 1 \qquad \text{probability } f_i e^{-\beta}, \tag{2}$$

$$n_i = 1 \;\rightarrow\; n_i = 0 \qquad \text{probability } f_i, \tag{3}$$

where we have set $J = 1$ and $\beta \equiv T^{-1}$. The non-trivial part of the dynamics is due to the facilitation function

$$f_i \equiv n_{i+1} + n_{i-1} - n_{i+1} n_{i-1}, \tag{4}$$

i.e., a spin flip on site $i$ can take place only if at least one if its nearest neighbours is in the excited state. Since

$f_i$ does not depend on $n_i$ then the time evolution of the model obeys detailed balance with respect to $H$ at temperature $\beta^{-1}$. The mean density of up spins in the equilibrium state is

$$c \equiv (1 + e^{\beta})^{-1}. \tag{5}$$

The unit of time is an MC sweep ($N$ attempted spin flips).

In the following, we consider an FA model in which $N$ is to be taken to infinity in the thermodynamic limit. We will take a subsystem of this model, containing $L+2$ spins, $\{n_0, \ldots, n_{L+1}\}$. The length $L$ is to remain finite: it is a mesoscopic quantity. A trajectory for the subsystem specifies the state of the $(L+2)$ spins at $Nt_{\rm obs}$ MC steps. The trajectory is defined within a spacetime observation box of size $Lt_{\rm obs}$. We consider observables such as the density of excitations within the box, for a given trajectory

$$m_{\rm traj} = (LNt_{\rm obs})^{-1} \sum_{i=1}^{L} \sum_{\tau=1}^{Nt_{\rm obs}} n_{i,\tau} \tag{6}$$

where $n_{i\tau}$ is the state of the $i$th spin in the $\tau$th state of the trajectory. Note that the boundaries $n_0$ and $n_{L+1}$ do not appear in the sum. As well as a measure of dynamical activity, $m_{\rm traj}$ is also a box magnetisation, by analogy with a spin system.

### A. Distribution of the magnetisation

We consider the distribution of the trajectory activity, or box magnetisation $m_{\rm traj}$:

$$P(m) = \sum_{\rm traj} P_{\rm traj} \delta(m - m_{\rm traj}). \tag{7}$$

The sum is over all possible trajectories of the system, with their associated probabilities $P_{\rm traj}$. In the limit of $L \to \infty$ or $t_{\rm obs} \to \infty$, the central limit theorem states that $P(m)$ will be sharply peaked around $m = c$, with a variance that scales as $(Lt_{\rm obs})^{-1}$. The observation of Ref. [3] was that, while this is the case in the limit of large $(Lt_{\rm obs})$, the distribution of $m$ remains non-trivial even for $L \gg \xi$ and $t_{\rm obs} \gg \tau$, where $\xi \approx c^{-1}$ and $\tau \approx c^{-3}$ are the correlation length and time associated with the zero temperature dynamical fixed point of this model.

We show various $P(m)$ in Fig. 3. The bulk of $P(m)$ is Gaussian, and this corresponds to trajectories like the one on the top-right of Fig. 1. The tails of $P(m)$ are exponential for $m$ small. This data was obtained using a combination of transition path sampling (TPS) [16] and umbrella sampling [17]. For details see the Appendix. The trajectories in the tail are dominated by rare large regions which have no excitations, like the the one on the bottom-right of Fig. 1.

To explain the presence of the exponential tail, suppose that we have a trajectory with an initial condition containing a large empty region of size $x$, and that

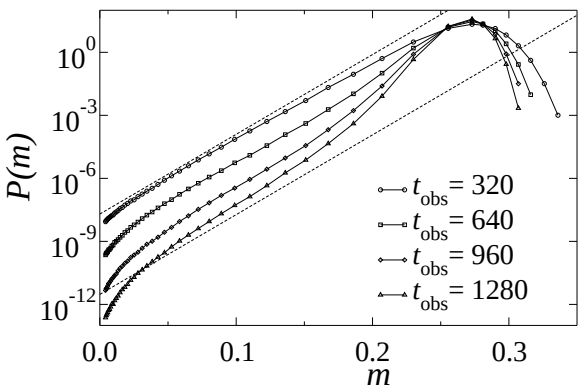


FIG. 3: Distribution of trajectory magnetization $P(m)$ at $\beta = 1$, $L = 60$ and various observation times. We use $N = 180$ which is large enough so that $P(m)$ does not depend on $N$. The exponential tails of $P(m)$ all have similar gradients: the dotted lines are $P(m) \sim \exp(\sigma m)$ with $\sigma = 87$.

this empty region persists throughout $t_{\rm obs}$, leading to a box magnetisation that is small. Now consider a trajectory whose initial condition has an empty region of size $x + (\Delta x)$, but is otherwise identical to the original one. Then the probabilities of the two trajectories are in the ratio $(1-c)^{\Delta x}$, and their magnetisations differ by approximately $c(\Delta x)/L$. Thus we predict

$$P(m) \sim (1-c)^{mL/c} = \exp[(mL/c)\ln(1-c)]. \tag{8}$$

The significance of this result is that the right hand side is independent of $t_{\rm obs}$: increasing the observation time changes the factor multiplying the tail in $P(m)$, but the gradient of the tail remains constant. Fig. 3 shows that the gradient is indeed independent of $t_{\rm obs}$. However, the quantitative prediction for its value is accurate only to within 20-30%. This inaccuracy arises because the large inactive region may extend beyond the edge of the box. Thus, adding extra down sites to the initial condition may decrease the magnetisation by an amount less than $(c/L)$.

In Fig. 3 the exponential tail of $P(m)$ depends only on $L$ and not on $t_{\rm obs}$, but this is a result of the shape of the observation box: the behaviour of $P(m)$ is symmetric with respect to $L$ and $t_{\rm obs}$. In Fig. 4 we show how $P(m)$ changes as we change the aspect ratio of the observation box. There is a crossover at $L \sim vt_{\rm obs}$, where $v \simeq 0.06$ at $\beta = 1$. For $L > vt_{\rm obs}$ the gradient of the exponential tail is independent of $t_{\rm obs}$ as described above, but for $L < vt_{\rm obs}$ then the argument must be modified. Typical trajectories at small $m$ change their form to that shown in Fig. 4 (right). In that case, increasing the width of the bubble does not change $m$; we must instead increase the time for which the inactive state persists. Repeating the argument leads to a situation in which the gradient of the exponential tail is proportional to $t_{\rm obs}$ and independent of $L$, see Fig. 4. In other words, the gradient of the exponential tail is proportional to $\max(L, vt_{\rm obs})$. The spatial

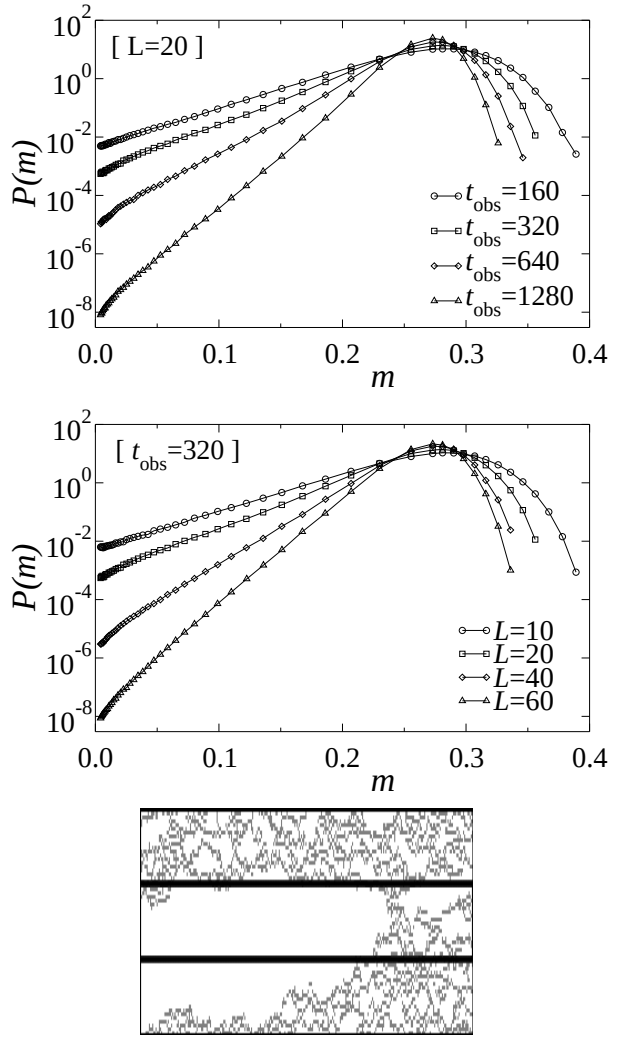


FIG. 4: We show $P(m)$ at $\beta = 1$ for varying $L$ and $t_{\rm obs}$. We use $N = \max(120, 3L)$ which is large enough that the results do not depend on $N$. (Top) Increasing observation time at at fixed $L = 20$. (Middle) Increasing box size $L$ at $t_{\rm obs} = 320$. As $L$ or $t_{\rm obs}$ is increased, we move from a regime in which the tail gradient is independent of the increasing parameter to a regime in which the gradient is proportional to that parameter. (Bottom) We show a typical trajectory for large $t_{\rm obs}$ and $L = 20$ where the observation box is outlined: the size of the total spatial region shown is $N = 60$. For large $L$ the trajectories are of the form shown in Fig. 1.

and temporal extent of the box enter on equal footing. The data of Fig. 4 is consistent with the crossover from large $L$ to large $t_{\rm obs}$ occuring when $t_{\rm obs}$ is of the order of the first passage time across a bubble of size $L$. This time scales as $(L/v) \sim (L/c^2)$ since the spreading velocity in the FA model is proportional to the branching rate, $c^2$.

Consistent with the known scaling of the FA model in one dimension [6], we find that the temperature dependent of $P(m)$ can be accounted for by using rescaled variables. The function

$$P(m/c; cL, c^3 t_{\rm obs}) \tag{9}$$

depends only weakly on $c$, as shown in Fig. 5. While subleading corrections to the scaling do appear to be significant, there is no qualitative change on lowering the temperature. This justifies our working at inverse temperatures around $\beta = 1$, where the data is easier to obtain than in the more glassy regime of the FA model ($\beta > 1$).

As a final observation in this subsection, we note that the behaviour of $P(m)$ for small observation boxes, $cL < 1$ or $c^3 t_{\rm obs} < 1$, is different from that for large boxes. This is shown in Fig. 6. The distribution acquires a secondary peak at $m \to 0$: there is a finite probability of observing $m = 0$, so that $P(m)$ diverges as $m \to 0$. We will return to this feature below.

### B. Comparison with a model of appearing and annihilating excitations (AA model)

In the previous subsection, the non-trivial structure in $P(m)$ occurs in the tails of the distribution. This behaviour is not linked to the universal critical correlations in the system, but rather to mesoscopic fluctuations. We will argue later that these rare mesoscopic fluctuations do contain significant information about the model. We first show explicitly the non-universality of the exponential tails of Figs. 3-5 by comparing $P(m)$ in the FA model with the AA model, which has the same critical scaling [8].

We define the AA model by specifying local moves for a chain of binary variables:

$$\begin{aligned}
(n_i, n_{i+1}) = (1,0) &\;\leftrightarrow\; (n_i, n_{i+1}) = (0,1), && \text{rate } \gamma e^{-\beta'} \\
(n_i, n_{i+1}) = (1,1) &\;\rightarrow\; (n_i, n_{i+1}) = (0,0), && \text{rate } \gamma \\
(n_i, n_{i+1}) = (0,0) &\;\rightarrow\; (n_i, n_{i+1}) = (1,1), && \text{rate } \gamma e^{-2\beta'}
\end{aligned}$$

where $\gamma = 2/(1 - e^{-\beta'})^2$ is an arbitrary temperature dependent factor that rescales the time, chosen for later convenience. These rates again respect detailed balance with respect to $H = \sum_i n_i$, and the inverse temperature is $\beta'$.

Correlation functions in the steady state of the AA model at a given temperature are related to those in the FA model at a different temperature [8] (strictly this holds when the facilitation function is proportional to the number of up neighbours, not when it is equal to zero or one as here, but there is no qualitative change to the physics). The relationship between correlators depends only on simple multiplicative factors, for example [8]

$$\begin{aligned}
&\langle n_{it} n_{jt'} \rangle_{{\rm FA},\beta} - \langle n \rangle^2_{{\rm FA},\beta} = \\
&\qquad \frac{4}{1 + e^{-\beta}} \left( \langle n_{it} n_{jt'} \rangle_{{\rm AA},\beta'} - \langle n \rangle^2_{{\rm AA},\beta'} \right),
\end{aligned} \tag{10}$$

where $\beta$ is the inverse temperature in the FA model and $\beta'$ the inverse temperature in the AA model. Equation (10) holds when

$$e^{-\beta'} = \frac{\sqrt{1 + e^{-\beta}} - 1}{\sqrt{1 + e^{-\beta}} + 1}. \tag{11}$$

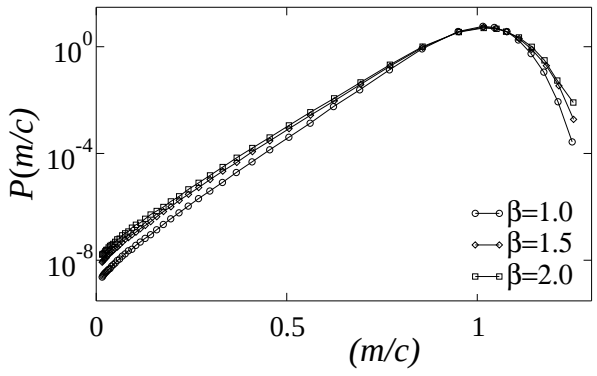


FIG. 5: Data showing (approximate) scaling of $P(m)$ in the FA model at various temperatures, scaled according to (9). We plot $P(m/c)$: the box sizes are $L = (60, 88, 135)$; the observation times are $t_{\rm obs} = (320, 1280, 5330)$; and we use $N = 3L$. These temperatures are not very small, so there are subleading corrections to scaling, but there is no qualitative change to the scaled distribution on lowering the temperature. Further, the computational time required at $\beta = 2$ is quite significant, so we cannot rule out small systematic errors arising from non-convergence of our TPS procedure (see appendix).

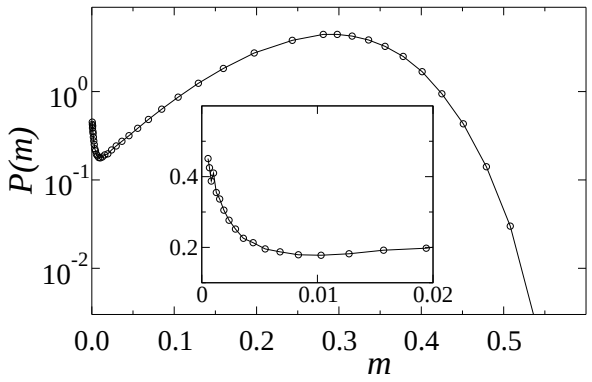


FIG. 6: Plot of $P(m)$ at $\beta = 1$, $L = 2$, $t_{\rm obs} = 160$, showing secondary maximum at small $m$. (Inset) Enlargement of the secondary peak, shown in a linear scale for $P(m)$.

It is clear from (10) that the scaling behaviour and critical properties of the FA and AA models are the same. However, their activity or magnetisation distributions are different, as shown in Fig. 7. The exponential tail is absent in the AA case. Moreover, the persistence functions of the two models are different [the persistence function is the probability that a site does not flip at all in an interval of length $t$]. The fluctuations responsible for the tails in $P(m)$ can be linked to the decoupling of exchange and persistence times in the FA model [18], a feature which is absent in the AA case. Both persistence functions and subsystem probability distributions are rather non-universal quantities, since they depend on the system at very many times. Further, we argue below that there are important differences between the FA and AA models: subsystem observables like $P(m)$ make these differences clear where two-point functions like $\langle n_{i\tau} n_{j0} \rangle$ do not.

## III. DYNAMICAL ACTION AND THERMODYNAMIC ANALOGY

We have shown that the distribution of subsystem magnetisations in the FA model has an exponential tail at small magnetisation. We also showed that this tail comes from rare mesoscopic regions of spacetime in which there are no up spins. In this section we study the statistical mechanics of the spacetime configurations of the subsystem. We draw an analogy between these spacetime statistics and the thermodynamic statistics of a system near a phase coexistence conditions.

To make this analogy concrete, we define the probability of a trajectory being generated by some (Markovian) dynamical rules:

$$P_{\rm traj} = \prod_{\tau=1}^{Nt_{\rm obs}-1} W(s_{\tau+1}|\{s_\tau, n_{0,\tau}, n_{L+1,\tau}\}) \times P_0(s_1) P_{\rm bc}(n_{0,t}, n_{L+1,t}), \quad (12)$$

where $s_\tau = \{n_{1\tau}, \ldots, n_{L\tau}\}$ represents the state of the system at time $\tau$; the transition probabilities are denoted by $W(s'|\{s, n_0, n_{L+1}\})$; $P_{\rm bc}(n_{0,t}, n_{L+1,t})$ is the probability of the trajectory of the two boundary spins; and $P_0(s_1)$ is the probability of the initial condition ($s_1$). We note that the transition probabilities into a state $s_{\tau+1}$ depend on the state of the boundary spins as well as the state $s_\tau$.

It is convenient to define the dynamical action:

$$\mathcal{E}_{\rm traj} = -\ln P_{\rm traj}. \quad (13)$$

However, we observe that the trajectory specifies the state of the system at $Nt_{\rm obs}$ time steps. As we take the limit $N \to \infty$, the probability of any specific trajectory vanishes (even though $L$ and $t_{\rm obs}$ are kept finite). (If a spin flips between times $t$ and $t'$ then it could flip on any of the extensive number of timesteps between these times. So the probability of any specific trajectory tends to zero as $N \to \infty$.) Taking the logarithm of a probability that is vanishing as $N \to \infty$ is a little problematic, but this is a familiar problem. For example, it arises in calculating the entropy of systems with continuous variables. The solution is that absolute values of the entropy (or action) depend explicitly on small coarse-graining scales that form part of their definitions.

Postponing this issue, the dynamical partition sum is

$$\mathcal{Z} = \sum_{\rm traj} e^{-\mathcal{E}_{\rm traj}} = 1. \quad (14)$$

The analogy with a thermodynamic partition sum should

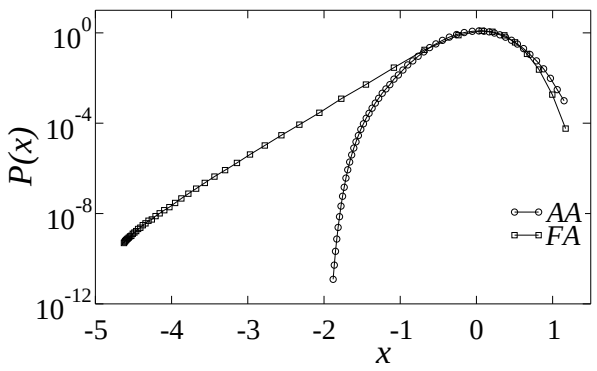


FIG. 7: Distribution of (reduced) box magnetization in the FA and AA models. The reduced variable $x = (m - \langle m \rangle)/\sigma_m$ where $\sigma_m^2 \equiv \langle (m - \langle m \rangle)^2 \rangle = c(1-c)L^{-1}$ is the variance of the instantaneous magnetisation. Parameters are $L = 60$, $t_{\rm obs} = 320$, $N = 180$; in the FA model $\beta = 1$; in the AA model $\beta'(\beta = 1)$ given by (11). For the AA model $P(m)$ is close to Gaussian. The standard deviation $\sigma_m$ is *not* trivially related to the variance of the box magnetisation, so the fact that the Gaussian parts of the two distributions are very similar is a non-trivial consequence of the exact mapping between the two models.

then be clear. We define

$$Z = \sum_{\rm conf} e^{-\beta U_{\rm conf}}, \tag{15}$$

where the sum is over configurations of a system; $U_{\rm conf}$ is the energy of a configuration; and $\beta$ is the inverse temperature. The free energy is $F(U)$

$$\begin{aligned} \beta F(U) &= -\ln[P(\beta U)] \\ &= -\ln[\sum_{\rm conf} e^{-\beta U_{\rm conf}} \delta(\beta U - \beta U_{\rm conf})]. \end{aligned} \tag{16}$$

The dynamical analogy of this quantity is then

$$\begin{aligned} \mathcal{F}(\mathcal{E}) &= -\ln[P(\mathcal{E})] \\ &= -\ln[\sum_{\rm traj} e^{-\mathcal{E}_{\rm traj}} \delta(\mathcal{E} - \mathcal{E}_{\rm traj})]. \end{aligned} \tag{17}$$

Having defined the dynamical action, we can now prove our assertion above that reducible partitions of the dynamics have equal free energies. If the dynamics are reducible into two partitions then we can write

$$\mathcal{Z} = P_{\rm ic}(1) + P_{\rm ic}(2) \tag{18}$$

where the two terms are the probabilities that an initial condition lies in one partition or the other. The difference in free energy density between the two phases will be

$$\mu = \lim_{N,t\to\infty} (Nt)^{-1} \log[P_{\rm ic}(1)/P_{\rm ic}(2)] \tag{19}$$

Finally, note that $P_{\rm ic}(1)$ and $P_{\rm ic}(2)$ represent probabilities of initial conditions, so their logarithms are at most $\mathcal{O}(N)$, and will be independent of $t$. Therefore the difference in free energy density vanishes in the limit of large time. This is the reason for the purely exponential tails in $P(m)$ observed in the previous section.

We now consider the distribution of the dynamical action in the FA model.

### A. Distribution of the dynamical action

For the FA model, we have

$$W(s_{\tau+1}|\{s_\tau, n_{0\tau}, n_{L+1,\tau}\}) = W_0 + \mathcal{P}_{s_{\tau+1},s_\tau} \frac{1}{N} \sum_{i=1}^{L} W_i \tag{20}$$

where the projector $\mathcal{P}_{s,s'}$ takes the value of unity if $s$ and $s'$ differ in the state of exactly one spin, otherwise it is equal to zero;

$$W_i = f_{i\tau}[(1 - n_{i,\tau+1})n_{i,\tau} + n_{i,\tau+1}(1 - n_{i\tau})e^{-\beta}] \tag{21}$$

accounts for transitions into state $s$; and

$$W_0 = \delta_{s_{\tau+1},s_\tau} \left\{ 1 - N^{-1} \sum_{i=1}^{L} \left[ f_{i\tau}(1 - n_{i\tau})e^{-\beta} + n_i f_{i\tau} \right] \right\} \tag{22}$$

accounts for transitions from state $s$. The symbol $\delta_{s,s'}$ is equal to unity if and only if states $s$ and $s'$ are identical, and the function $f_{i\tau}$ was defined in (4): its value is unity if spin $i$ is free to flip; otherwise it is zero. These operators enforce the constraint that only one spin flips on each time step.

Taking the limit of large $N$, and using (13), we arrive at the action for an allowed trajectory:

$$\begin{aligned} \mathcal{E}_{\rm traj}^{(N)} &= \mathcal{N}_{\rm upflips} \ln(Ne^{\beta}) + \mathcal{N}_{\rm downflips} \ln(N) \\ &\quad -N^{-1} \sum_{\tau=1}^{Nt_{\rm obs}} \sum_{i=1}^{L} f_{i\tau}[(1 - n_{i\tau})e^{-\beta} + n_{i\tau}] \\ &\quad +(\text{boundary terms}), \end{aligned} \tag{23}$$

where $\mathcal{N}_{\rm upflips} = \sum_{i\tau} n_{i,\tau+1}(1 - n_{i\tau})$ is the total number of flips from state 0 to state 1 inside the observation box and, similarly, $\mathcal{N}_{\rm downflips} = \sum_{i\tau}(1 - n_{i,\tau+1})n_{i\tau}$ is the number of flips from 1 to 0. Of course, trajectories containing transitions that are not allowed by the dynamical rules have $P_{\rm traj} = 0$ and their action is formally infinite; we ignore them in what follows. As noted above, the probability of any trajectory vanishes as $N \to \infty$, so we must introduce a coarse-graining timescale $\delta t$. We define

$$\tilde{P}_{\rm traj} = \sum_{{\rm traj}'(\delta t)} P_{{\rm traj}'} \simeq (N\delta t)^{\mathcal{N}_{\rm upflips} + \mathcal{N}_{\rm downflips}} P_{\rm traj}, \tag{24}$$

where the sum is over trajectories with the same spin flips as the original trajectory, but the flips may happen within an interval $(\delta t)$ of their original times. The second,

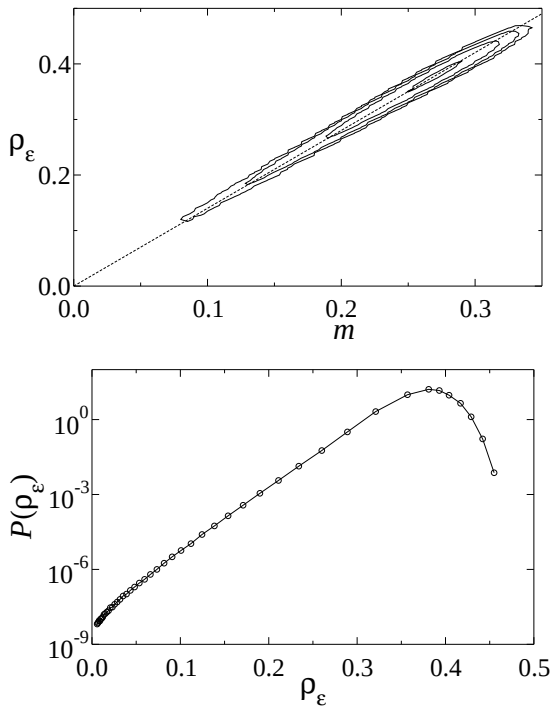


FIG. 8: Distribution of the action in the FA model for $L = 60$, $t_{\rm obs} = 320$, obtained with $N = 180$. (Top) Contour plot of the joint probability distribution for action density and magnetisation $P(\rho_{\mathcal{E}}, m)$ (obtained from $2 \times 10^7$ independent trajectories). The contours are at $P(m, \rho_{\mathcal{E}}) = 10^3, 10, 0.1, 2 \times 10^{-3}$. The dotted line is the prediction (33). (Bottom) Distribution of the action density $P(\rho_{\mathcal{E}})$ [where $\rho_{\mathcal{E}} = \mathcal{E}/(Lt_{\rm obs})$].

approximate, equality indicates that as long as $(\delta t)$ is not too large then the probability of all trajectories in the sum will be approximately equal, and the number of such trajectories is $(N\delta t)^{\mathcal{N}_{\rm flips}}$. The result is that

$$\begin{aligned}\mathcal{E}^{(\delta t)}_{\rm traj} &\equiv -\ln \tilde{P}_{\rm traj} \\ &= \mathcal{N}_{\rm upflips} \ln(1/e^{-\beta}\delta t) + \mathcal{N}_{\rm downflips} \ln(1/\delta t) \\ &\quad + N^{-1} \int_0^{t_{\rm obs}} {\rm d}\tau \sum_{i=1}^{L} f_{i\tau}[(1-n_{i\tau})e^{-\beta} + n_{i\tau}] \\ &\quad + (\text{boundary terms}), \end{aligned} \tag{25}$$

where we have converted the sum to an integral, which is valid in the limit of large $N$. This definition of the action is parametrised by the coarse-grained time scale $(\delta t)$. Typical values of $\mathcal{E}^{(\delta t)}_{\rm traj}$ are independent of $N$ and extensive in $L$ and $t_{\rm obs}$. Our results do not depend qualitatively on $\delta t$; the numerical results below are at $\delta t = 1$. Finally, we have no prescription for calculating the boundary terms in the action; we expect these to be small, so we neglect them in what follows.

To relate the distribution of the action to the distribution of activity or magnetisation, note that facilitated spins in the FA model (those with $f_i = 1$) equilibrate quickly. We define the density of facilitated spins in a trajectory to be

$$n_{\rm f} = (LNt_{\rm obs})^{-1} \sum_{\tau}^{Nt_{\rm obs}} \sum_{i=1}^{L} f_{i\tau}. \tag{26}$$

Assuming that the facilitated spins are equilibrated, we expect

$$(LNt_{\rm obs})^{-1} \sum_{\tau}^{Nt_{\rm obs}} \sum_{i=1}^{L} f_{i\tau}(1-n_{i\tau}) \simeq (1-c)n_{\rm f}, \tag{27}$$

$$(LNt_{\rm obs})^{-1} \sum_{\tau}^{Nt_{\rm obs}} \sum_{i=1}^{L} f_{i\tau} n_{i\tau} \simeq c n_{\rm f}, \tag{28}$$

$$\mathcal{N}_{\rm upflips} \simeq \mathcal{N}_{\rm downflips} \simeq cLt_{\rm obs} n_{\rm f}, \tag{29}$$

where the approximate equalities indicate that the joint distribution of each pair of observables will be sharply peaked around these values (see Fig. 8). Further, we expect

$$n_{\rm f} \simeq m(2-c), \tag{30}$$

where the approximate equality holds in a similar sense, and $m$ is the magnetisation or activity of a trajectory, defined in (6). We define the joint distribution of the action density $\rho_{\mathcal{E}}$ and the magnetisation by

$$P(\rho_{\mathcal{E}}, m) = \sum_{\rm traj} \tilde{P}_{\rm traj} \delta(m - m_{\rm traj})\, \delta[\rho_{\mathcal{E}} - (\mathcal{E}^{(\delta t)}_{\rm traj}/Lt_{\rm obs})]. \tag{31}$$

We show $P(\rho_{\mathcal{E}}, m)$ in Fig. 8, along with the probability distribution of $\rho_{\mathcal{E}}$,

$$P(\rho_{\mathcal{E}}) = \int {\rm d}m\, P(\rho_{\mathcal{E}}, m). \tag{32}$$

As expected, we find that the joint distribution is sharply peaked around

$$\rho_{\mathcal{E}} = mc(2-c)\left[2 + \beta - 2\ln(\delta t)\right]. \tag{33}$$

We conclude that the exponential tail in the magnetisation distribution is intrinsically linked with the exponential tail in the distribution of the dynamical action.

### B. Spacetime thermodynamics

We motivated our discussion of the dynamical action by analogy with a thermodynamic free energy. We now discuss our results in terms of this analogy.

The trajectories of Fig. 1 show that a typical region with relatively small magnetisation is a large inactive "bubble". While true for the FA model, this is not the case for the AA model, nor for models of non-interacting random walkers. In those models, trajectories with small magnetisations do not have segregated regions of large and small magnetisations; rather, they have a uniform

reduction in the density across the subsystem. These models also lack exponential tails in $P(m)$, see Fig. 7. This important difference between the FA and AA models arises from the presence of an empty absorbing state in the FA model that is absent in the AA model. We see that despite their identical scaling and two point equilibrium correlations, the FA and AA models do permit very different behaviour in certain multi-point observables.

The exponential tails in $P(m)$ reflect an apparent stability of bubbles of the inactive phase. It is useful to think in terms of phase coexistence between a metastable inactive phase and a stable active one. The metastability of the inactive phase is a result of the fact that there are no transitions into or out of a state in which the spins are all down. Consider the (dynamical) free energy for droplets of the absorbing phase with linear size $l$ and temporal extent $\tau$. That is, define the $P_{\rm bubble}(l,\tau)$ of Eq. (1) to be the total statistical weight of all trajectories with such an inactive region centred at the origin.

For observation windows such that $vt_{\rm obs} < L$, the magnetisation of a box with a single large bubble is

$$m \simeq c[1-(l/L)]. \tag{34}$$

The probability of a bubble of width $l$ that spans the temporal extent of the box is

$$P(l) \simeq \int_{t_{\rm obs}}^{\infty} {\rm d}\tau\, P(l,\tau). \tag{35}$$

Assuming that $\Lambda$ is large, so that $P(l,\tau)$ is sharply peaked around $l = v\tau$, then

$$\frac{\rm d}{{\rm d}m} \ln P(m) \simeq (L/c)\left[\sigma_1 + (\sigma_2/v) + 2(\mu/v)L(1-m/c)\right], \tag{36}$$

for $m < c[1-(vt_{\rm obs}/L)]$. Unless $\mu$ is very small, the term proportional to $\mu$ will dominate at large $L$, leading to a Gaussian distribution. However, in the case of small $\mu$, the distribution is exponential in $m$, and the gradient of this exponential tail is proportional to $L$ and independent of $t_{\rm obs}$, as observed in Fig. 3. A similar argument holds in the opposite regime of $L < vt_{\rm obs}$ and $m < c[1-(L/vt_{\rm obs})]$, which explains the exponential tails of Fig. 4.

We conclude that a bubble free energy of the form

$$F_{\rm bubble}(l,\tau) = \sigma_1 l + \sigma_2 \tau + \mu l\tau + \Lambda(l-v\tau)^2 \tag{37}$$

with $\mu \to 0^+$ explains the subsystem distributions for the FA model. (Of course, we must have $\mu > 0$ since otherwise the inactive phase would be thermodynamically stable, which is not the case.) The scaling of the data indicates that $\sigma_1 \sim \sigma_2/v \sim c$ and $v \sim c^{-2}$. In our thermodynamic analogy this corresponds to the situation near a phase coexistence boundary, in which the free energy of bubbles of the metastable phase are dominated by their surface energies. The smallness of $\mu$ results from the proximity to phase equilibrium in $(d+1)$-dimensional spacetime.

Pursuing this analogy, we identify the two parameters associated with phase coexistence. The dynamical activity, or excitation density, of the active phase is $\langle m\rangle = c$. The typical lengthscale associated with the bubbles is $\sigma_1^{-1}$ which scales as $c^{-1}$. Thus, the typical bubble size and the typical spacing between up spins are scaling in the same way as the temperature is reduced. This is a consequence of detailed balance in the FA model, which implies that excitations are uncorrelated at equal times: $\langle (n_{i\tau}-c)(n_{j\tau}-c)\rangle = c(1-c)\delta_{ij}$.

In the next section, we show how generalising the FA model to a system which does not obey detailed balance leads to a situation in which the typical bubble sizes are larger than the excitation spacing. This new situation is the usual one in systems at phase coexistence: we show that the FA model is rather special case, because of the extra symmetry of detailed balance.

## IV. GENERALISED MODEL

The thermodynamic analogy described above leads to an interesting question: what is the analogy of the temperature parameter $\beta$ in the dynamical system? By analogy with (16), we define:

$$\begin{aligned} b\mathcal{F}_b(\mathcal{E}) &= -\ln[P_b(b\mathcal{E})] \\ &= -\ln[\sum_{\rm traj} e^{-b\mathcal{E}_{\rm traj}}\delta(b\mathcal{E}-b\mathcal{E}_{\rm traj})]. \end{aligned} \tag{38}$$

Then we identify a new ensemble in which the probabilities of trajectories are

$$P_{b,{\rm traj}} = \mathcal{Z}_b^{-1} e^{-b\mathcal{E}_{\rm traj}}, \tag{39}$$

where $\mathcal{Z}_b^{-1} = \sum_{\rm traj} P_{b,{\rm traj}}$. This ensemble has the action distribution

$$-\ln P_b(\mathcal{E}) = -[\ln P_{b=1}(\mathcal{E}) + (b-1)\mathcal{E}]. \tag{40}$$

Hence, if $P_{b=1}(\mathcal{E})$ has an exponential tail with gradient $\sigma$ then $P_b(\mathcal{E})$ has a similar exponential tail with the reduced gradient $\sigma-(b-1)$. Since the magnetisation and action are tightly correlated, the distribution of the magnetisation also has an exponential tail with reduced gradient. As $b$ is increased, the gradient of this tail vanishes. We associate this vanishing with the proliferation of trajectories with large bubbles. In [3] it was argued that this proliferation would appear as a first order transition to a state with large inactive bubbles, if an appropriate dynamics could be found to generate the $b$-ensemble.

However, any dynamics that realises the $b$-ensemble is unphysical, in the sense that the transition probabilities depend explicitly on the size of the spacetime box, and on the position (and time) within it. However, there is a way to generate a similar effect in a fashion that does not have this effect. Suppose we reduce the probability of all trajectories in our original (FA, $b=1$) ensemble, according to their magnetisation (total number of excitations).

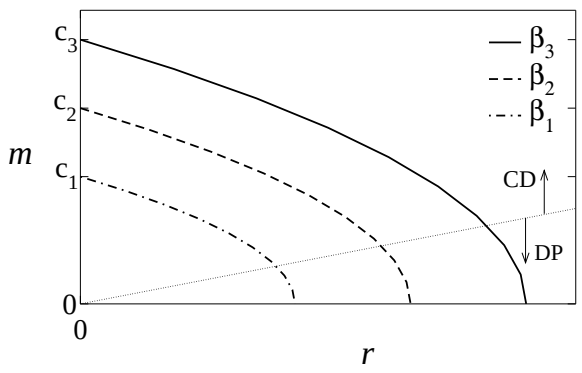


FIG. 9: Sketch of the steady state density in the generalised model, as a function of $r$, for different values of $\beta$ with $\beta_1 > \beta_2 > \beta_3$. The axis $r = 0$ is the FA model and the axis $m = 0$ is a line of critical points. The dotted line separates the region in which DP scaling will apply from those in which $r$ can be treated perturbatively [so the scaling will be that of the coagulation-diffusion (CD) fixed point]. The FA model ($r = 0$) is the unique case for which the critical scaling is coagulation-diffusion; for finite $r$ the relevant critical point is DP.

This is achieved by introducing an extra process whereby up spins can flip down, even when unfacilitated. Having reduced the probability of all trajectories in the old ensemble, we add new trajectories that were not allowed before (these are the trajectories containing unfacilitated down flips).

For the trajectories that were allowed in the FA model we will have

$$\begin{aligned} P_{b,\mathrm{traj}} &\propto \exp(-\mathcal{E}_{\mathrm{traj}})\exp(-rLt_{\mathrm{obs}}m_{\mathrm{traj}}) \\ &\simeq \exp(-b\mathcal{E}_{\mathrm{traj}}), \end{aligned} \tag{41}$$

where the second approximate equality follows because of the strong correlations between $S_{\mathrm{traj}}$ and $m_{\mathrm{traj}}$, and we have $(b-1) \simeq rLt_{\mathrm{obs}}\langle m/\mathcal{E}\rangle$. Hence this procedure should mimic the effect of increasing $b$.

We implement this procedure by supplementing the FA model with the additional dynamical process

$$1_i \to 0_i \qquad \text{probability } (1-f_i)r. \tag{42}$$

Note that $r = 0$ is the FA model. For $r > 0$ then the system no longer obeys detailed balance, and $\beta$ can no longer be interpreted as an inverse temperature. (We require $r \geq 0$ since all probabilities must be positive.) The introduction of the new "death" process for up spins allows the possibility of a dynamical transition at finite branching rate, which will be in the directed percolation (DP) universality class [9].

The qualitative behaviour of the model with finite $r$ is shown in Fig. 9. The "dimensionless" parameter that determines the effective size of $r$ is the product of the death rate and the relaxation time of the FA model:

$$r\tau \simeq re^{3\beta} \equiv R, \tag{43}$$

which defines $R$. At any finite $\beta$ there is a directed percolation transition to an active state that we expect to occur when $R$ is of order unity. This transition is accompanied by a diverging static correlation length:

$$\langle n_{i\tau}n_{j\tau}\rangle - \langle n_{i\tau}\rangle^2 \sim e^{|r_i-r_j|/\xi_{\mathrm{DP}}}, \tag{44}$$

where $\xi_{\mathrm{DP}}$ is the length scale that diverges at the transition. On the other hand, if $R = 0$ then there is a transition at $c = 0$ that is controlled by the coagulation-diffusion fixed point. In that case we have

$$\langle n_{i\tau}n_{j\tau}\rangle - \langle n_{i\tau}\rangle^2 \sim \delta_{ij}. \tag{45}$$

for all $c$. We show in the figure how the crossover into the DP critical region is always relevant if $R$ is finite, but does not affect the behaviour if $R = 0$. We note that between two and four dimensions a similar picture holds, but the scaling at $R = 0$ will be Gaussian [8].

We now consider the action distribution in the models with finite $r$. The probabilities of allowed trajectories satisfy

$$\begin{aligned} -\ln P_{b,\mathrm{traj}} \;=\; & \mathcal{N}_{\mathrm{upflips}}\ln(Ne^{\beta}) \\ & +\mathcal{N}^{(\mathrm{fac})}_{\mathrm{downflips}}\ln N + \mathcal{N}^{(\mathrm{death})}_{\mathrm{downflips}}\ln(N/r) \\ & +N^{-1}\sum_{\tau,i} f_{i\tau}[(1-n_{i\tau})e^{-\beta} + n_{i\tau}(1-r)] \\ & +N^{-1}\sum_{\tau}\sum_{i} rn_{i\tau}, \end{aligned} \tag{46}$$

where $\mathcal{N}^{(\mathrm{fac})}_{\mathrm{downflips}} = \sum_{i\tau} f_{i\tau}(1-n_{i\tau+1})n_{i\tau}$ is the number of facilitated flips from 1 to 0, and $\mathcal{N}^{(\mathrm{death})}_{\mathrm{downflips}} = \sum_{i\tau}(1-f_{i\tau})(1-n_{i\tau+1})n_{i\tau}$ is the number of unfacilitated down flips.

Comparing (46) with (23), there are three new terms: the last term is the correction ($rmLt_{\mathrm{obs}}$) which reweights the trajectories in the original ensemble according to (41). The term proportional to the number of death events vanishes for trajectories in the original ensemble, but is significant for typical trajectories in the new ensemble. It reflects the fact that the ensemble of trajectories with finite $r$ is only an approximation to the one defined in (39). Finally, there is a small correction to the penultimate term that arises from the fact that the death process affects only unfacilitated spins.

By analogy with (25) we define

$$\begin{aligned} \mathcal{E}^{(r)}_{\mathrm{traj}} &= \mathcal{N}_{\mathrm{upflips}}\ln(e^{\beta}) + \mathcal{N}^{(\mathrm{death})}_{\mathrm{downflips}}\ln(1/r) \\ &+ \int_0^{t_{\mathrm{obs}}} \mathrm{d}\tau \sum_i \left\{ f_{i\tau}[(1-n_{i\tau})e^{-\beta} + n_{i\tau}(1-r)] + n_{i\tau}r \right\}, \end{aligned} \tag{47}$$

where we have set the coarse-graining time scale $\delta t = 1$ for ease of writing. We expect equations (27-30) to remain true since facilitated spins are still equilibrated at a density close to $c$ (but note that the mean density in

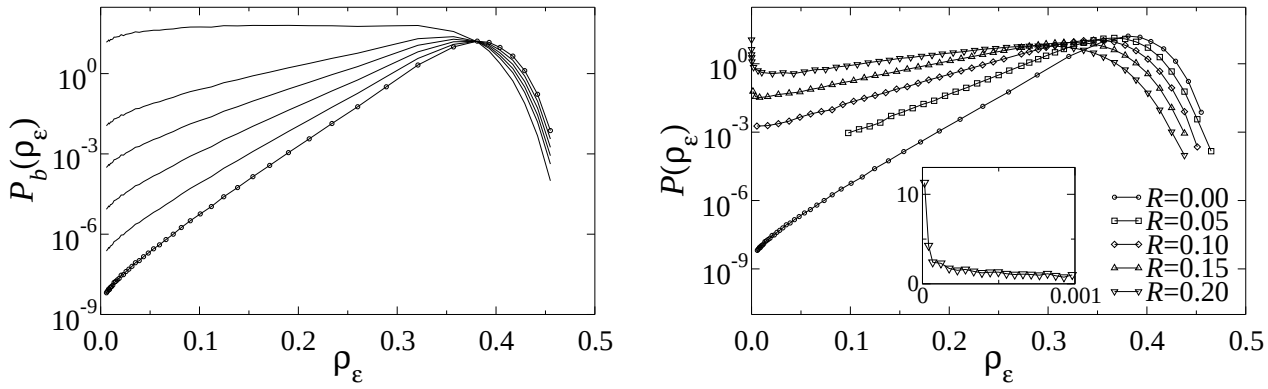


FIG. 10: (Left) Action distribution in the ensemble with finite $b = (1.0, 1.005, 1.001, 1.0015, 1.002, 1.003)$. The distribution at $b = 1$ is that of Fig. 8 and is shown with symbols. To get data at $b > 1$ we simply use (40) and rescale by a constant for convenience (this data is shown as simple lines). [We reiterate that there is no physical model that realises this ensemble.] (Right) Action distribution with varying $R$ at $L = 60$, $t_{\rm obs} = 320$, $\beta = 1$. For $R > 0$ we use $N = 6L = 360$ to ensure that data is independent of $N$. The behaviour at small $R$ is qualitatively similar to the behaviour at small $b$ in that the gradient of the exponential tail decreases; at larger $R$ a secondary minimum appears. The inset shows an expanded view of the secondary minimum that is present at $R = 0.2$. Samples with the action exactly equal to zero are omitted from the plot: the probability of this happening is of the order of 1% at $R = 0.2$.

the system will be less than $c$: the death process reduces the mean density). To estimate the contribution of the new terms, we note that

$$\mathcal{N}^{(\rm death)}_{\rm downflips} \;\simeq\; mrLt_{\rm obs}, \tag{48}$$

which shows that the typical trajectories at finite $r$ differ from those of the FA model in that they have a finite (albeit small) density of death events.

In Fig. 10 we plot the distribution of the action density at finite $r$ and compare it with the behaviour of the $b$-ensemble. Since the system does not obey detailed balance the TPS procedure becomes inefficient: data at finite $r$ is obtained by simple binning and histogramming. We show that introducing the death process mimics the $b$-ensemble, at least for small $R$ and small $b$. We find that the gradient of the exponential tail decreases quickly, while the mean density of excitations decreases more slowly. In the language of section III, increasing $r$ leads to a reduction in the active state density $\langle m\rangle$, combined with a reduction in the "surface energies" $\sigma_1$ and $\sigma_2$. If we reduce the temperature in the FA model ($r = 0$, $c \to 0$) we have $\sigma_1 \sim c$ and $\langle m\rangle \sim c$, so the typical bubble size $\sigma_1^{-1}$ scales in the same way as the inverse density of up spins. On the other hand, as we approach the DP fixed point ($\beta$ finite, $r \to r_{\rm crit}$) then we expect

$$\sigma_1 \sim (r - r_{\rm crit})^{\nu_{\rm DP}}, \qquad \langle m\rangle \sim (r - r_{\rm crit})^{\beta_{\rm DP}} \tag{49}$$

where $(\nu_{\rm DP}, \beta_{\rm DP}) \simeq (1.1, 0.3)$ are the exponents of the DP fixed point [9] ($\beta_{\rm DP}$ should not be confused with the parameter $\beta$ that enters the transition probabilities). On approach to criticality the mean bubble size increases much faster than the inverse density since $\nu_{\rm DP} > \beta_{\rm DP}$. The up spins cluster together, leaving large inactive regions consisting only of down spins. Introducing the death process drives the system towards a phase separation into active and inactive regions of spacetime. This can be seen in the trajectories of Fig. 11.

As we increase $R$ and approach the DP critical point, the situation differs from that at finite $b$. We observe a crossover when the typical size of inactive regions exceeds the observation box ($\sigma_1 L \sim 1$). In that case, $P(\mathcal{E}_r)$ acquires a second peak at zero magnetisation (see the largest value of $R$ in Fig. 10). This is analogous to the situation for small boxes ($cL < 1$) in the FA case (recall Fig. 6). In the thermodynamic language, it corresponds to a second minimum in the free energy, as would be expected near a first order phase transition. Here, the phase transition is second order, but the finite size of the observation box means that we observe apparently first-order behaviour: the divergence of the correlation length is cut off at the size of the observation box.

We have shown that adding a death process to the FA model strengthens the analogy between trajectory statistics and the statistical mechanics of phase coexistence. This death process, which breaks microscopic reversibility, can be thought of as a scheme for "driving" of the FA model. Excitations are removed, in a way that spoils detailed balance, so one can think of it as a "thickening" process in analogy with what occurs in driven dense soft materials (see e.g. [19]). In the FA model, the only length scale is the inverse density of up spins; if $r$ is finite then a new length scale appears: the DP correlation length. This allows the density of active regions to decouple from their separation, leading to richer behaviour than that of the FA model (which corresponds to the particular case of the phase coexistence in which the two length scales are equal).

Throughout this article, we have emphasised the broad applicability of the idea of spacetime phase coexistence

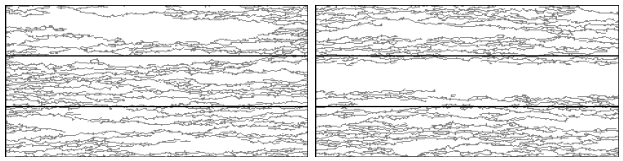

FIG. 11: Sample trajectories at $R = 0.1$ with conditions otherwise similar to Fig. 3 ($\beta = 1$, $L = 60$ $t_{\rm obs} = 320$). (Left) Sample from centre of distribution. (Right) Sample with $m_{\rm traj} \sim \langle m \rangle/2$. Clearly there are more large inactive regions in these trajectories than in those of Fig. 1; increasing $R$ from zero leads to proliferation of large "bubbles".

by focussing on general features of the models, such as microscopic reversibility and reducibility of the dynamics. We expect the behaviour described here to be generic in kinetically constrained models with reducible dynamics [6, 12, 20, 21, 22]. More generally, the extent to which this behaviour can be observed in physical (atomistic) glass-formers remains an important question.

### Acknowledgments

We thank Mauro Merolle for discussions. This work was supported by NSF grant CHE-0543158 (RLJ); EPSRC grants no. GR/R83712/01 (RLJ and JPG) and GR/S54074/01 (JPG), University of Nottingham grant no. FEF 3024 (JPG), and by the US Department of Energy Grant no. DE-FG03-87ER13793 (DC).

## APPENDIX A: TRANSITION PATH SAMPLING

We calculated probability distributions for various observables in the FA model: these were obtained by a combination of transition path sampling (TPS) [16] and umbrella sampling [17]. Here we give a brief description of the procedure used.

Transition path sampling is a Monte Carlo procedure applied to trajectories of a dynamical system (a trajectory is a particular realisation of the dynamics). We use it to efficiently sample restricted ensembles of trajectories. The procedure is well-established [16], but we present some information regarding its application to the FA model for completeness.

Suppose that we wish to sample trajectories with magnetisation $m$ smaller than some reference value $m_1$. The simplest way to do this is to generate statistically independent trajectories, accepting only those that satisfy the restriction $m < m_1$. However, if $m_1$ is much smaller than the mean of $m$ then this is inefficient.

Instead, we can generate unbiased trajectories satisfying the restriction by deforming a set of initial trajectories, as long as the deformations satisfy detailed balance with respect to the probability distribution within the constrained ensemble of trajectories. Such deformations are called TPS moves. One possibility is to take a trajectory of length $t_{\rm obs}$ and keep only the part with $t < (xt_{\rm obs})$ with $0 < x < 1$; we the generate the rest of the trajectory using the dynamical rules prescribed for the system (we use a continuous time Monte Carlo algorithm [23]). If the new trajectory has $m < m_1$ then it replaces the old one; otherwise the move is rejected and we retain the old trajectory. This is a "shooting" move [16]. We couple this the move with the reverse procedure in which we discard the part of the trajectory with $t > (xt_{\rm obs})$ and regenerate the rest of the trajectory by propagating backwards in time (since we have detailed balance then the steady state of the FA model is invariant under time-reversal, so this is a valid way to generate unbiased trajectories).

In addition to these moves, we also use "shifting" moves [16] in which we shift the trajectory in time, discarding the parts of the new trajectory with $t < 0$ or $t > t_{\rm obs}$. We then regenerate the remaining parts of the new trajectory. We find that this combination of moves is quite efficient for exploring the restricted ensembles of interest.

## APPENDIX B: UMBRELLA SAMPLING

We use umbrella sampling [17] to calculate probability distributions by measuring ratios such as

$$P_{i,i+1} = \frac{P(m < m_{i+1})}{P(m < m_i)} \tag{B1}$$

where $m_i$ and $m_{i+1}$ are two cutoffs for the variable $m$ with $m_{i+1} < m_i$.

Consider an ensemble of all allowed trajectories for the system, with their statistical weights. In order to measure $P_{i,i+1}$ we sample a restricted ensemble which contains only trajectories with $m < m_i$; these trajectories have the same weights as they would have in the original ensemble. We then measure the probability that $m < m_{i+1}$ within the restricted ensemble: this probability is equal to $P_{i,i+1}$.

Our procedure is as follows:

1. Start with a representative set of trajectories from the unrestricted ensemble.

2. Choose an ordered set of cutoff magnetisations ($m_1 > m_2 > \cdots > m_p$) for which we will calculate the probabilities $P_{i,i+1}$.

3. Explore the unrestricted ensemble, measuring the fraction of trajectories with $m < m_1$. (This is done by sampling independent trajectories.)

4. Once we have a good enough estimate for $P(m < m_1)$, start a restricted ensemble with trajectories satisfying $m < m_1$. Typically we store $N_e = 100$ such trajectories.

5. Explore the restricted ensemble using TPS, measuring the fraction of trajectories with $m < m_2$. Typically this takes $N_m = 100 - 10000$ TPS moves per ensemble member.

6. Once we have a good enough estimate for $P_{12}$, we discard all trajectories with $m > m_2$ and replace them by trajectories with $m < m_2$. These trajectories are generated by continuing the TPS procedure and accepting all trajectories that satisfy the new constraint. The resulting set of trajectories are not statistically independent so we equilibrate the new ensemble by allowing it to evolve from the biased initial condition. Typically we use around $N_m$ TPS moves per ensemble member. We test for equilibration by tracking the fraction of trajectories with $m < m_3$, since this will be the quantity that we will measure on the next step.

7. We then repeat steps 5 and 6 for increasingly restricted ensembles. At each step, we measure $P_{i,i+1}$.

Once we have the $P(m < m_1)$ and the set of $P_{i,i+1}$ then it is simple to reconstruct the probability distribution of the observable $m$.


[1] For reviews see: M.D. Ediger, C.A. Angell and S.R. Nagel, J. Phys. Chem. **100** 13200 (1996); C.A. Angell, Science **267**, 1924 (1995); P.G. Debenedetti and F.H. Stillinger, Nature **410**, 259 (2001).

[2] For reviews see: H. Sillescu, J. Non-Cryst. Solids **243**, 81 (1999); M.D. Ediger, Annu. Rev. Phys. Chem. **51**, 99 (2000); S.C. Glotzer, J. Non-Cryst. Solids, **274**, 342 (2000); R. Richert, J. Phys. Condens. Matter **14**, R703 (2002); H. C. Andersen, Proc. Natl. Acad. Sci. U. S. A. **102**, 6686 (2005).

[3] M. Merolle, J. P. Garrahan, and D. Chandler, Proc. Natl. Acad. Sci. U. S. A. **102**, 10837 (2005).

[4] D. M. Huang and D. Chandler, Phys. Rev. E **61**, 1501 (2000).

[5] M. Clusel, J. Y. Fortin, and P. C. W. Holdsworth, Phys. Rev. E **70**, 046112 (2004).

[6] F. Ritort and P. Sollich, Adv. Phys. **52**, 219 (2003).

[7] G. H. Fredrickson and H. C. Andersen, Phys. Rev. Lett. **53**, 1244 (1984).

[8] R. L. Jack, P. Mayer, and P. Sollich, J. Stat. Mech. (2006), P03006.

[9] H. Hinrichsen, Adv. Phys. **49**, 815 (2000).

[10] J. P. Garrahan and D. Chandler, Phys. Rev. Lett. **89**, 035704 (2002).

[11] P. Harrowell, Phys. Rev. E **48**, 4359 (1993).

[12] J. P. Garrahan and D. Chandler, Proc. Natl. Acad. Sci. U. S. A. **100**, 9710 (2003).

[13] Y. J. Jung, J. P. Garrahan, and D. Chandler, Phys. Rev. E **69**, 061205 (2004).

[14] C. Toninelli, M. Wyart, L. Berthier, G. Biroli, and J. P. Bouchaud, Phys. Rev. E **71**, 041505 (2005).

[15] E. Bertin, J. P. Bouchaud, and F. Lequeux, Phys. Rev. Lett. **95** (2005).

[16] P. G. Bolhuis, D. Chandler, C. Dellago, and P. L. Geissler, Ann. Rev. Phys. Chem. **53**, 291 (2002).

[17] D. Frenkel and B. Smit, *Understanding molecular simulation* (Academic Press, 2001).

[18] Y. Jung, J. P. Garrahan, and D. Chandler, J. Chem. Phys. **123**, 084509 (2005).

[19] C. B. Holmes, M. E. Cates, M. Fuchs, and P. Sollich, J. Rheol. **49**, 237 (2005).

[20] S. Eisinger and J. Jackle, J. Stat. Phys. **73**, 643 (1993).

[21] L. Berthier and J. P. Garrahan, J. Phys. Chem. B **109**, 6916 (2005).

[22] W. Kob and H.C. Andersen, Phys. Rev. E **48**, 4364 (1993); J. Jäckle and A. Krönig, J. Phys. Condens. Matter **6**, 7633 (1994); A.C. Pan, J.P. Garrahan and D. Chandler, Phys. Rev. E **72**, 041106 (2005); C. Toninelli, G. Biroli and D.S. Fisher, J. Stat. Phys. **120**, 167 (2005); C. Toninelli, G. Biroli and D.S. Fisher, Phys. Rev. Lett. **96**, 035702 (2006).

[23] M. E. J. Newman and G. T. Barkema, *Monte Carlo Methods in Statistical Physics* (Oxford University Press, 1999).